jmb Article

Surface Growth of a Motile Bacterial Population Resembles Growth in a Chemostat

Daniel A. Koster, Avraham Mayo, Anat Bren and Uri Alon

Department of Molecular Cell Biology, *Weizmann Institute of Science, Rehovot 76100, Israel*

Correspondence to Daniel A. Koster and Uri Alon: *daniel.koster@weizmann.ac.il; uri.alon@weizmann.ac.il*
http://dx.doi.org/10.1016/j.jmb.2012.09.005
Edited by I. B. Holland

Abstract

The growth behavior in well-mixed bacterial cultures is relatively well understood. However, bacteria often grow in heterogeneous conditions on surfaces where their growth is dependent on spatial position, especially in the case of motile populations. For such populations, the relation between growth, motility and spatial position is unclear. We developed a microscope-based assay for quantifying *in situ* growth and gene expression in space and time, and we observe these parameters in populations of *Escherichia coli* swimming in galactose soft agar plates. We find that the bacterial density and the shape of the motile population, after an initial transient, are constant in time. By considering not only the advancing population but also the fraction that lags behind, we propose a growth model that relates spatial distribution, motility and growth rate. This model, that is similar to bacterial growth in a chemostat predicts that the fraction of the population lagging behind is inversely proportional to the velocity of the motile population. We test this prediction by modulating motility using inducible expression of the flagellar sigma factor FliA. Finally, we observe that bacteria in the chemotactic ring express higher relative levels of the chemotaxis and galactose metabolism genes *fliC*, *fliL* and *galE* than those that stay behind in the center of the plate.

Introduction

In laboratory studies, bacterial cultures are usually shaken to create a homogeneous environment that is convenient for experimental study.[1] However, bacterial populations in nature are often spread over a surface in the form of colonies, swarms or biofilms.[2–6] These bacterial populations are heterogeneous in space in terms of their gene expression and growth.[5,7,8] Bacterial colonies on hard surfaces typically grow at the edges where nutrients are available.[2] On the other hand, motile and chemotactic populations use chemotaxis to explore new areas rather than rely only on growth and diffusion.[9] Although the growth and gene expression of shaken cultures and immobile colonies have been extensively investigated, the growth laws and gene expression of swimming colonies have been less studied. Examples of questions that remain unanswered include: do chemotactic populations grow exponentially in time, linearly or similar to growth in a chemostat where bacterial growth and outflow are balanced? Does the entire chemotactic population participate in growth or only a part of the population? Bacteria may chemotax to obtain nutrients and it is thus expected that chemotaxis increases growth. However, the precise relation between the chemotactic velocity, growth rate and the spatial distribution of the population is largely unknown.

In this study, we investigate bacterial growth and gene expression in chemotactic populations in space and time. We developed a novel microscope-based assay to quantify *in situ* bacterial growth, motility and promoter activity at the population level across a surface at high temporal resolution and accuracy. As a model system, we

observe a population of *Escherichia coli* that grows and performs chemotaxis through soft agar plates[10] with galactose as a carbon source and a chemoattractant. Soft agar plates have been used to study chemotaxis receptor signaling.[11–13] In the simplest form of the assay, bacteria are typically deposited in the center of a soft agar plate (the inoculum), after which the bacteria consume a chemoattractant, creating a spatial gradient. The bacteria then simultaneously consume and chase the chemoattractant outward and form a migrating ring made of bacteria. In more complex media, multiple rings form one after the other where each ring contains bacteria that chase another chemoattractant. For example, in a tryptone soft agar plate, at least three rings form that, in order of appearance, perform chemotaxis toward serine, aspartic acid and threonine. Keller and Segel have developed a theoretical framework for chemotaxis of bacterial populations. Many studies have adapted the framework to model a variety of experimental scenarios, including growth,[14,15] non-growth conditions,[16] chemotaxis toward an excreted chemoattractant,[17] varying gel concentration[18] and various forms for the chemotactic and growth terms, reviewed by Tindall *et al.*[19]

Previous studies using soft agar plates[18,20] found that the velocity of the rings is constant in time and is insensitive to the agar concentration up to ~0.25% (w/v). Furthermore, it has previously been established that for the rings to migrate, bacteria need to grow and be motile.[20] The efficiency with which *E. coli* navigates through the agar maze is dependent on their tumbling frequency: bacteria that incessantly tumble and thus constantly change direction do not get far, while bacteria that tumble infrequently get stuck in the agar cavities and do not spread through the gel efficiently.[20]

Here, we use a microscopy assay to make several new findings on the dynamics and gene expression of bacteria in the swim plate. The origin of the swim ring is in the center rather than at the edges of the inoculum. After an initial transient, the density and shapes of the ring remain constant in time. Some bacteria are left behind the ring, forming a plateau region of constant cell density in space with no cell growth. The results suggest that the chemotactic population grows similar to bacterial growth inside a chemostat—with constant inflow of nutrient and constant outflow of cells. We test a prediction of this chemostat model, namely, that velocity of the ring is inversely proportional to the height of the plateau region of bacteria left behind the ring, by varying bacterial velocity using the controlled expression of the flagella sigma factor FliA. We also find exponentially growing, linearly growing and stationary populations, as well as differential expression across space of key genes in the relevant metabolic and chemotaxis pathways.

Results

Microscopy assay for bacterial density and gene expression in space and time

We study soft agar plates in which a population of bacteria performs chemotaxis toward a single carbon source (D-galactose). The plate is viewed under a microscope (Fig. 1a) enclosed in an incubator at a constant temperature of 37 °C. We use 6-well soft agar plates, where each well contains *E. coli* reporting for a different gene from a GFP (*g*reen *f*luorescent *p*rotein)-promoter library[21] (Fig. 1b). Each well is scanned in transmission (Fig. 1c) and fluorescence (Fig. 1d), after which the fields of view are stitched together to produce a continuous image of the plate. A radially averaged profile is computed, reporting on bacterial density and accumulated fluorescence (GFP) expression from the promoter under investigation (see Materials and Methods for more information).

Different growth phases coexist in different regions—exponential, linear and stationary

The microscopy assay reveals several phases in the spatiotemporal development of the bacterial population. First, bacteria deposited in the center multiply using galactose as a carbon source and start to appear as a dark spot (Fig. 2a; $t=6$ h). After a few hours, depending on initial conditions, the galactose gradient that the bacteria create is sufficiently strong for a front of bacteria to start chasing galactose in all directions. Growth and chemotaxis occur simultaneously. The front advances at a constant velocity (Fig. 2b) of approximately 480 μm/h, depending on conditions, consistent with previous measurements,[10,18,20] while its shape remains constant (full width at half-maximum = 410 ± 40 μm, $n=5$; Fig. 2b, inset). As we increase the galactose concentration in the medium, exit from the drop region is delayed but the velocity and spatial profile of the ring are unaffected. A variant of the Keller–Segel model[22,23] that includes bacterial diffusion, growth and chemotaxis, as well as galactose metabolism and diffusion, produces a sharp bacterial front that advances at a constant velocity, in agreement with our experimental observations (Fig. 3a).

To ask how bacterial growth depends on space, we divide the plate into a "drop region" (red region in Fig. 2a) and an expanding "ring region" (purple region in Fig. 2a). Figure 3b shows two radially averaged bacterial density profiles. To quantify growth, we calculate the number of bacteria n at time point t in a region between radii r_1 and r_2 by computing the integral under the bacterial density curve, $n(t) = \int_{r_1}^{r_2} r\rho(r,t)\,dr$, where $\rho(r,t)$ is the bacterial

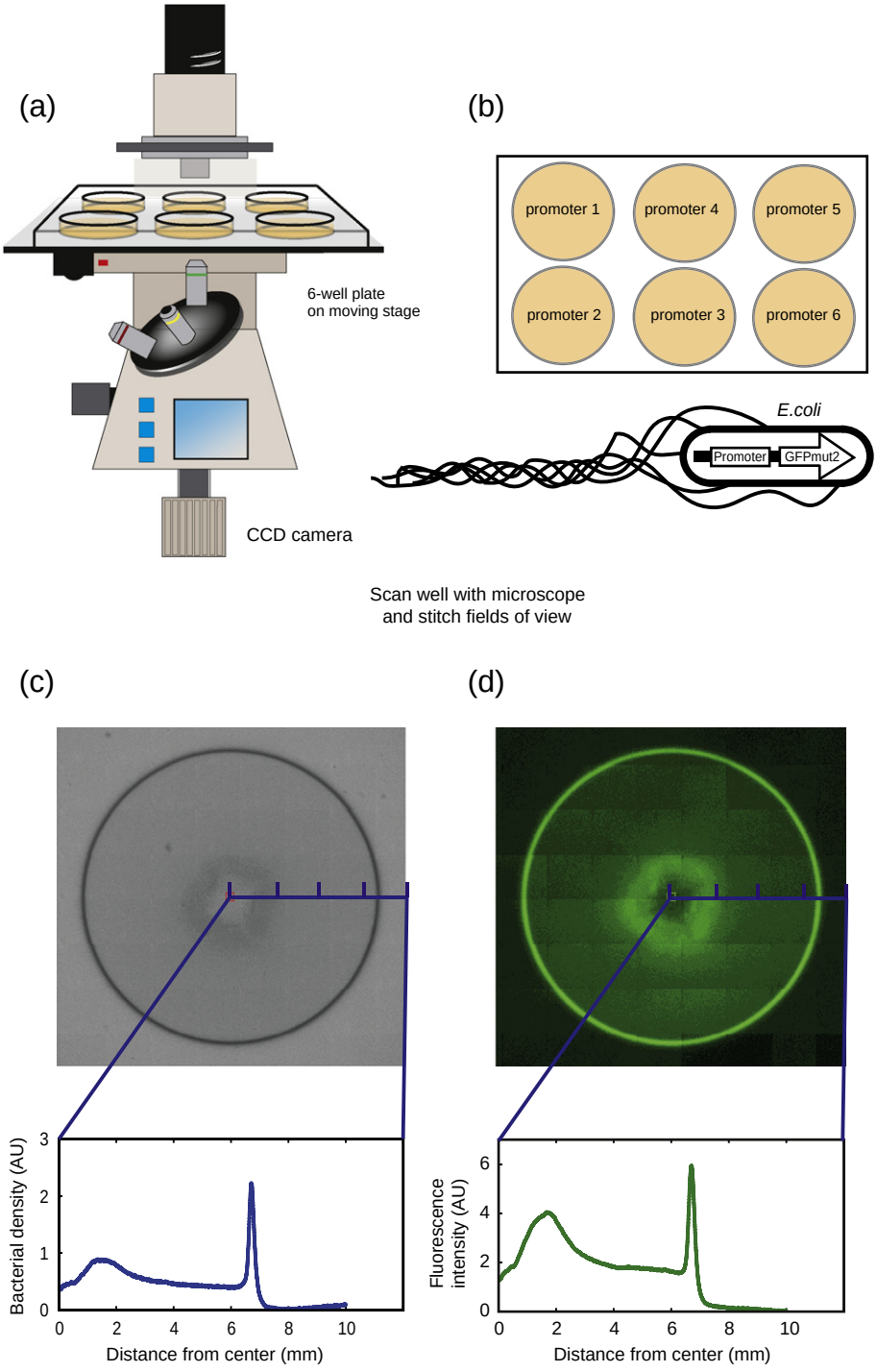

Fig. 1. Experimental strategy to measure bacterial density and gene expression on a surface. (a) An inverted microscope scans a 6-well plate that is mounted on a moving stage. (b) Each well contains an inoculum of *E. coli* RP437 carrying a low-copy reporter plasmid, where the promoter under investigation drives the expression of a fast-folding GFP. In transmission (c), dark regions report density of bacteria, and in fluorescence (d), bright regions report on accumulated GFP from the promoter. The radial profile is obtained by averaging 100 independent measurements along the contour.

density profile across the plate. The drop region is defined between $r_1 = 0$ mm (the center of the plate) and $r_2 = 1.2$ mm. Because the ring moves, its values for r_1 and r_2 are not fixed and are defined at half-peak maximum. When considering growth in space, we distinguish between increase in bacterial density and

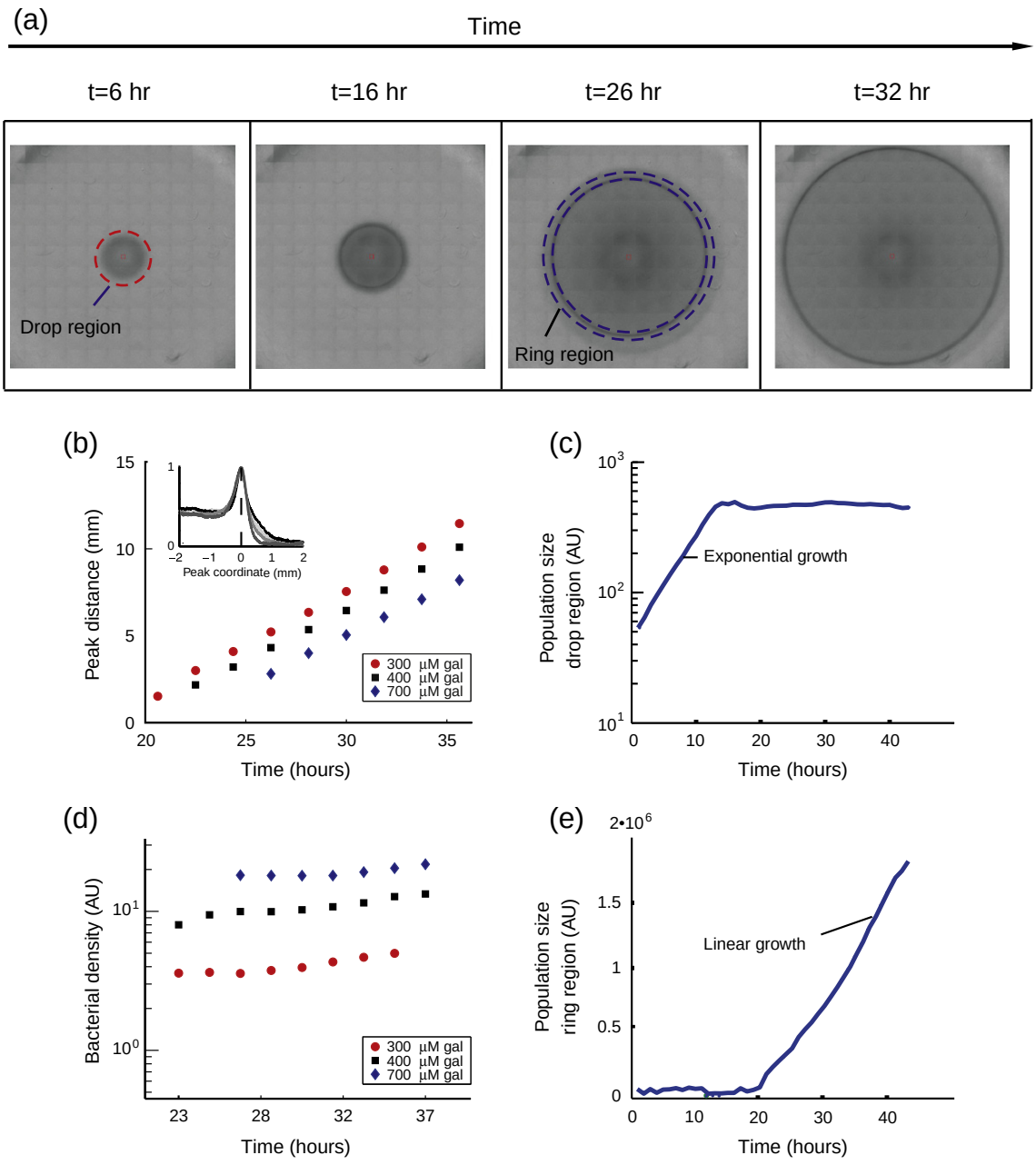

Fig. 2. The spatiotemporal developement of a bacterial population in a swim plate. (a) Images from a time-lapse movie showing growth in the "drop region" (red), where the bacteria are initially deposited, followed by the outward advance of a bacterial ring that performs chemotaxis up a self-created galactose gradient. (b) The velocity of the advancing ring is constant with time and insensitive to the galactose concentration. As the ring advances, the shape of its density profile and its width remain constant, as shown by shifting different profiles to have the same peak position (inset). (c) Prior to exiting the drop region, bacteria grow exponentially. (d) The bacterial density in the expanding ring is approximately constant with time. It increases with increasing nutrient concentration (error between day-to-day repeats about 10%). (e) The bacterial population in the ring grows linearly in time because its density remains constant in time and its area scales linearly with its radius.

increase in the total population size. For shaken cultures in a fixed volume V, this distinction is irrelevant and density and population size are simply related by $n(t)=\rho(t)V$. Growth in the drop region is similar to growth in a fixed volume in the sense that the region size is constant over time; the bacteria are not yet chemotactic and diffuse only slowly in comparison to the timescale of the experiment. As a function of time, the bacterial density in this region increases exponentially

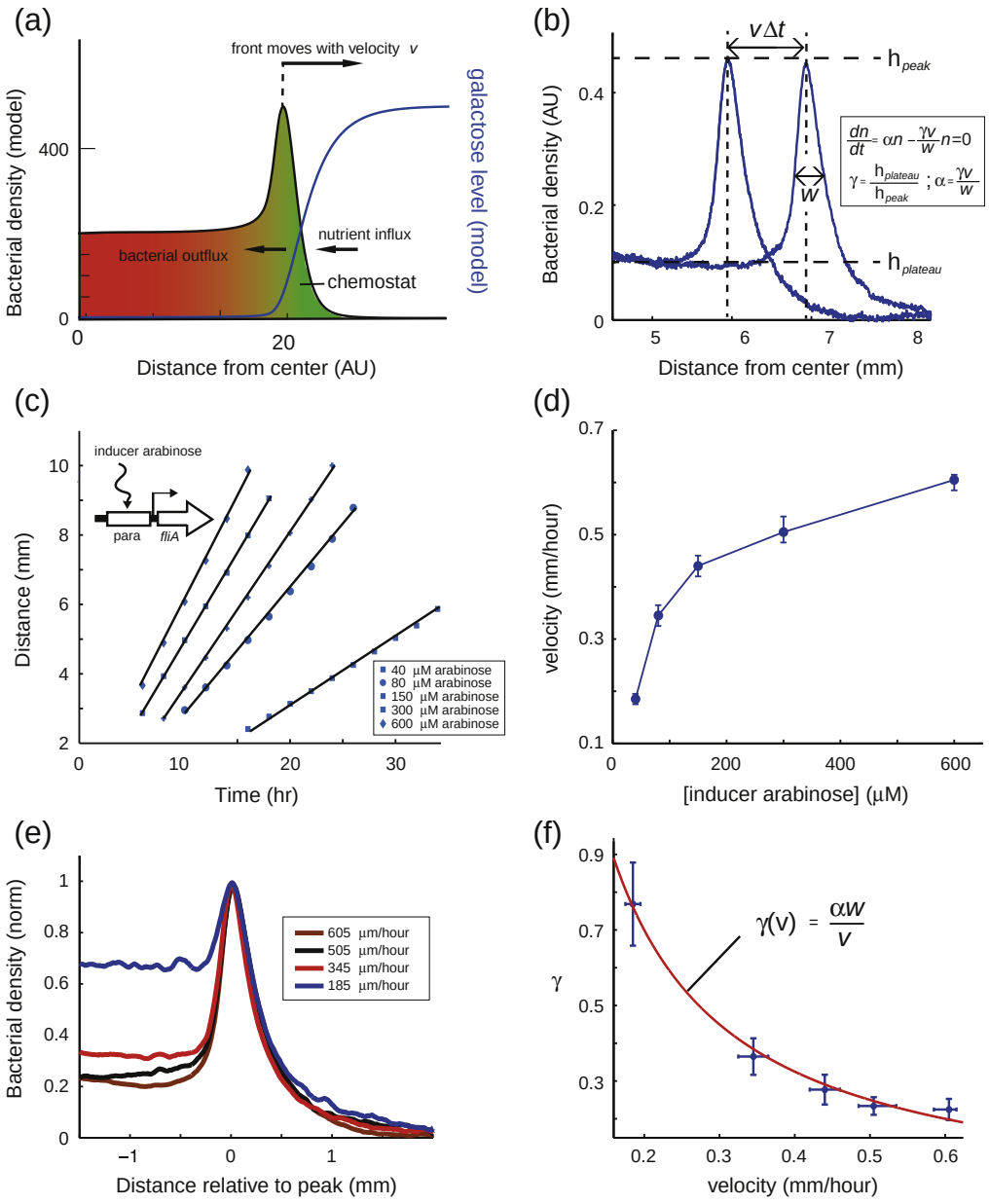

Fig. 3. (a) Modeled bacterial density and galactose profile from a Keller–Segel type model.[23] The front moves with velocity v and provides nutrients to the bacterial population in the ring. The chemostat region in which bacteria grow is shown in green. Part of the advancing population is lost, leading to the formation of a plateau of bacteria that do not grow (red region). (b) Two bacterial density profiles measured at Δt time intervals. Within the peak, with width w, bacteria grow at specific growth rate α. As the chemotactic population migrates with velocity v, bacteria are left behind and form a plateau with height $h_{plateau}$. The fraction of the chemotactic population that is lost, γ and is defined as $h_{plateau}/h_{peak}$. (c and d) Increasing the inducer concentration in the medium leads to an increase in the migration rate of the chemotactic population through the gel in the *ara*$^-$ RP437Δ*fliA*Δ*flgM* strain containing a plasmid carrying *fliA* under the control of the arabinose promoter. (e) As the velocity is decreased, the density in the plateau region becomes higher. (f) The waste fraction γ and the chemotactic velocity are inversely proportional, in support of the chemostat model. Error bars in γ represent the standard deviation (over $n=5$ time-points); error bars in the velocity measurement come from the fit of the distance *versus* time data to a linear relation.

(Fig. 2c) until, at 12 h, the number of bacteria saturates. Then, a ring that starts to travel outward and remains at constant bacterial density in time is formed (Fig. 2d). The population size in the ring increases linearly with time (Fig. 2e). This is because the area of a ring grows linearly with its radius. As the galactose concentration is increased, the bacterial density in the ring increases (Fig. 2d).

Bacteria in the ring region exhibit chemostat-like growth

We now consider the mode of growth of the mobile ring population and consider the influence of chemotaxis and the spatial distribution of the population. Our data show that as the bacterial ring advances in space, a plateau of bacteria forms behind the advancing ring [Figs. 1c and d, 2b (inset) and 3b]. Such a plateau is found in some Keller–

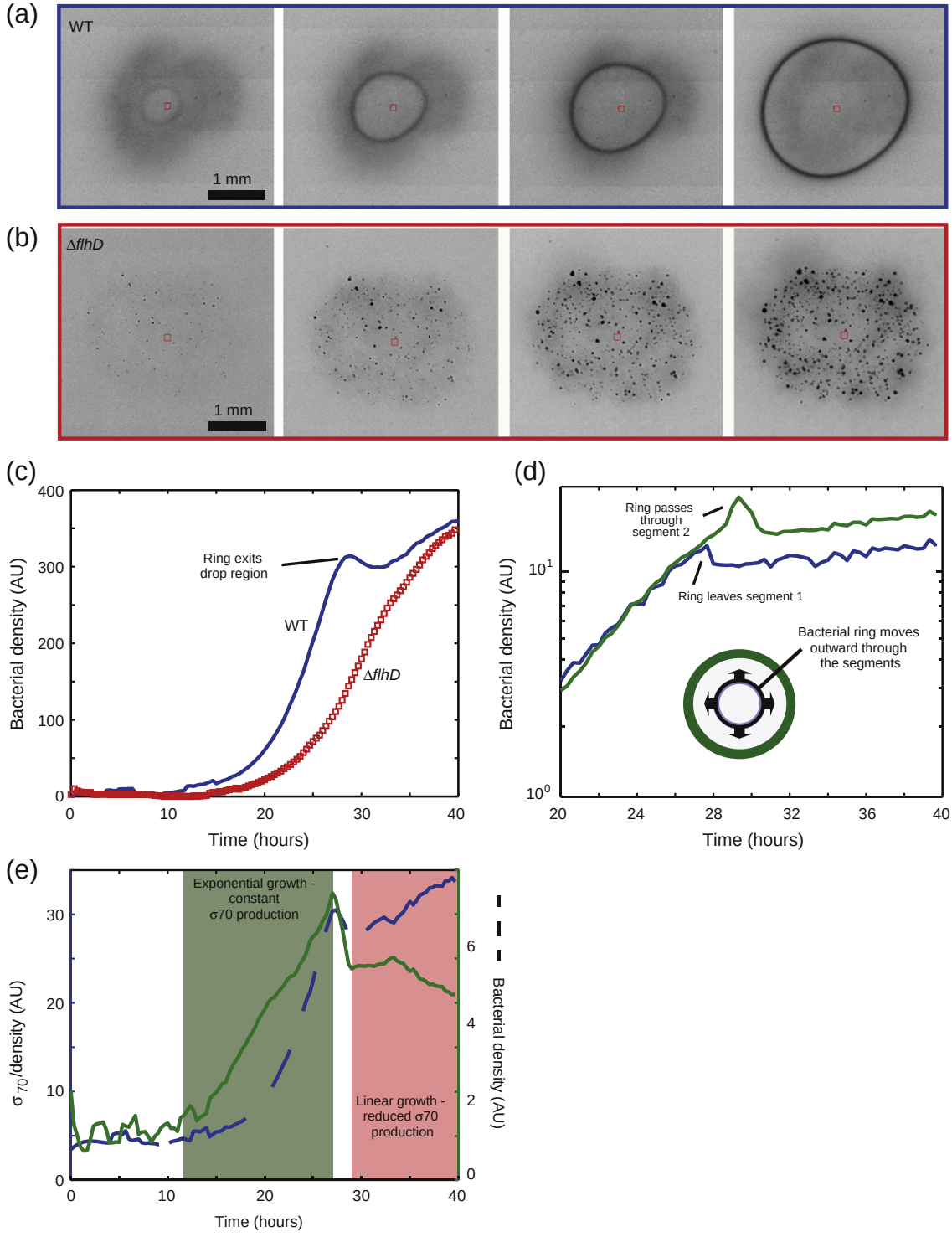

Fig. 4 (*legend on next page*)

Segel type models[18] but has not been reported in quantitative swim plate experiments. We find that the height of this plateau does not change with time (Fig. 3b), suggesting that bacteria in this region do not grow, presumably because the carbon source galactose has been depleted behind the advancing ring.[10] Indeed, we found that the amino acids in the medium required by strain RP437 do not support detectable growth without additional carbon sources. We therefore conclude that the bacteria in the plateau region originate from the ring population and are "left behind" by the advancing ring.

The presence of a plateau of "waste" bacteria, together with our observation that the bacterial density at the peak is constant with time, leads us to propose that the bacteria in the advancing ring grow similar to growth in a chemostat (Fig. 3a). Bacteria in a chemostat grow in a vessel to which nutrients are continuously added. The inflow of medium to the vessel is balanced by the outflow of waste (medium and bacteria).[24] In analogy to the chemostat, new nutrients are continuously added to the ring population because of the chemotaxis toward galactose. Similar to the waste of a chemostat, bacteria are continuously removed from the back part of the ring population, where the gradient is too shallow to sustain sufficient chemotaxis velocity. Because the ring advances at a constant velocity and the shape of the peak is invariant, bacteria in the ring obtain new nutrients at a constant rate and bacteria are left behind at a constant rate.

In a regular chemostat at steady-state, the rate of change in the number of bacteria n is given by $dn/dt=\alpha n-(m/V)n=0$. The growth rate is given by $\alpha=m/V$, where m is the flow-in rate of fresh medium and V is the volume of the vessel. Similarly, for the expanding chemotactic ring, we can write $dn/dt=\alpha n-(\gamma v/w)n=0$ and $\alpha=\gamma v/w$, where v is the velocity of the ring, w is its width and γ is a dimensionless factor describing the "waste fraction" of the spatial chemostat and that we define as the ratio between the height of the plateau and the height of the peak $h_{plateau}/h_{peak}$ (Fig. 3b). According to this model, the growth rate of the chemotactic population is related to both the chemotactic velocity of the population and its distribution in space. Plugging in typical values ($w=410\,\mu m$, $v=480\,\mu m/h$ and $\gamma=0.3$; see below), we obtain $\alpha\approx 0.35\,h^{-1}$ compared to $0.5\pm 0.02\,h^{-1}$ for the bacterial growth rate in bulk culture. The bacterial growth rate is slightly higher if one takes into account the fact that the area of the ring increases linearly (Fig. S1).

A prediction of the proposed spatial chemostat growth model is that, under otherwise identical growth conditions, increasing the chemotactic velocity would alter the spatial distribution of the population (specifically γ and w), according to $\alpha=\gamma v/w$. To test this prediction, we modulate the chemotactic velocity by controlling levels of the flagella sigma factor FliA expressed under the arabinose-inducible araBAD promoter.[25] We measure the spatial distribution (γ and w) of the ring population as a function of the ring velocity v. The *E. coli* strain RP437 is unable to utilize arabinose for growth.[26] Control experiments show that arabinose does not significantly affect the ring velocity of RP437. To exclude interference of background levels of chromosomal FliA, we use RP437 deleted for the *fliA* gene, RP437Δ*fliA*Δ*flgM*.

Figure 3c and d shows that increasing inducer levels leads to an increase in the chemotactic velocity of the ring through the gel. When increasing the velocity, we make two observations: (i) w remains constant and (ii) the height of the plateau decreases (Fig. 3e). To test the relation between v, w and γ quantitatively, we plot γ against v (Fig. 3f) and find that $\gamma(v)=\frac{a}{v}+c$ describes the data well (the red line in Fig. 3f is the model with best-fitted parameters: $a=\alpha w=0.15\pm 0.02\,mm/h$ and $c=-0.05\pm 0.05$). With $a=0.15$ and $w=0.41\,mm$, we obtain $\alpha=0.36\pm 0.16\,h^{-1}$, close to the value found above. The data are described well using a fixed value for α, which is interesting because it implies that, under the present conditions, the cost of flagella production is

Fig. 4. The interaction between mobile and immobile populations in the drop region. (a) Time-lapse movie of the drop region for WT *E. coli* RP437. The dark region represents the growing bacteria in the inoculum. From the center, a ring advances outward toward the boundaries of the drop region. (b) The behavior of a non-flagellated mutant RP437 (Δ*flhD*) differs from WT in that growth takes place within the micro-cavities of the gel from which the nonmotile bacteria are unable to escape.[20] No chemotactic ring forms. (c) Growth curves for WT (blue) and mutant (Δ*flhD*) RP437 within the perimeter of the drop area. Exit of the chemotactic ring from the drop region corresponds to a decrease in bacterial density (around $t=29\,h$). (d) Growth curves from two 250-μm segments within the drop region show the interaction between the moving ring and the population that does not take part in chemotaxis. The ring forms in segment 1 and, at $t=28$, it leaves the segment, leading to a decrease in bacterial density. Approximately 1 h later, the density of segment 2 rises and drops due to the passage of the ring through the segment. (e) Information about the physiological state of the motile and nonmotile populations is gleened from GFP levels driven by a σ_{70}-dependent promoter. Both the exponentially rising bacterial density in the drop region (blue broken line) and the expression levels from the σ_{70} promoter per density (green continuous line) that rises are indicative of growth (green block). However, as the ring passes through the segment (decrease in density at $t=27\,h$), expression levels of the σ_{70} promoter cease to rise and even decline, consistent with entry into stationary phase (red block).

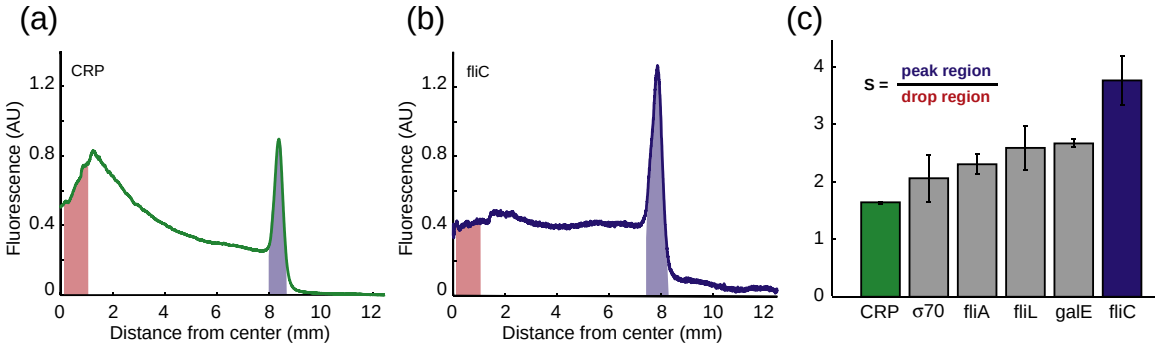

Fig. 5. Differential gene expression across the plate. Expression of the CRP reporter (a) and of the *fliC* (flagellin) promoter (b) is not equally distributed in space. (c) Quantification (the parameter *s* represents the ratio of integrated fluorescence in the peak and drop regions) shows that the flagellar and galactose genes are expressed at higher levels in the ring than in the drop. The parameter *s* is the ratio between the area under the fluorescence curve in the ring region and the drop region. Error bars represent the standard deviation between day-to-day repeats.

negligible. Indeed, a more complex *v*-dependent cost function that takes into account a production cost,[27] for example, $\alpha(v) = \alpha - \frac{\delta v}{1 - v / v_{max}}$, does not improve the fit. We conclude that the bacteria in the chemotactic ring grow similar to a spatial chemostat with a growth rate that is slightly lower than the maximum growth rate in a batch culture.

The swim ring begins within the inoculum, not at its edges

We next focused on the beginning of the swim ring process. We asked whether the ring starts at the edges of the inoculum or, instead, it originates from its inner parts. For this purpose, we measured the "drop region" at an increased time resolution of 15 min to observe transient waves of bacteria. Figure 4a and b shows the spatiotemporal development of a WT (*w*ild-*t*ype) bacterial population and an *flhD* mutant population that is incapable of synthesizing flagella. While the WT population grew dispersed over the inoculation region and formed a ring that expanded from the center outward, non-flagellated bacteria were trapped in the agar cavities and failed to form a motile ring.[20]

The exit of WT bacteria from the drop region was manifested in the growth curve (Fig. 4c, blue line) by a decrease in bacterial density that was not observed in the mutant strain (red line). We divided the region into two thin 250-μm-wide segments, one corresponding to the inside and the other corresponding to the edge of inoculum, and measured growth curves in each segment (Fig. 4d). The bacterial population in the inner segment (blue curve in Fig. 4d) grew exponentially until, at t=28 h, the ring forms and leaves the segment, causing a decrease in bacterial density, after which the remaining population saturated. In the outer segment (green), which is further away from the center, the population grew exponentially until the ring arrives (at t=29 h), causing a sudden increase in density followed by a decrease when it leaves, after which the population again saturated. We conclude that the ring starts inside the inoculum, not at its edges, and travels through the inoculum outward.

We next ask how the advancing chemotactic ring interacts with the population in the inoculum that remains stationary. In each segment of the inoculum, we test the growth state of the cells by measuring GFP expression from a synthetic promoter with a concensus σ_{70} binding site. This reports on growth without the interference of system-specific transcription factors.[28] Figure 4e shows that the bacterial density (blue broken line) grows exponentially (green block) and that the σ_{70} reporter intensity increases (continuous green line), indicative of vigorous growth. However, as soon as the ring leaves (at t=29 h), GFP levels from the σ_{70} promoter abruptly remain constant, indicating a halt in production from the σ_{70}-dependent promoter consistent with entry into stationary phase. The advancing chemotactic population depletes the remaining population of nutrients, forcing them into stationary phase.

Differential gene expression across space

We measured the spatial distribution of the promoter activity of five operons relevant for the process of chemotaxis toward galactose: *fliL* (the promoter of the *fliLMNOPQR* operon[29] that encodes biosynthesis proteins of the flagella), *fliA* (the flagella-specific sigma factor gene σ_{28}[30,31]), *fliC* (the flagellin gene, encoding the protein that makes up the flagella; because it is solely transcribed using σ_{28}, it also functions as a reporter for σ_{28} levels[32]), a synthetic promoter that reports on σ_{70} levels[28] and that is used to probe the growth state of the bacteria

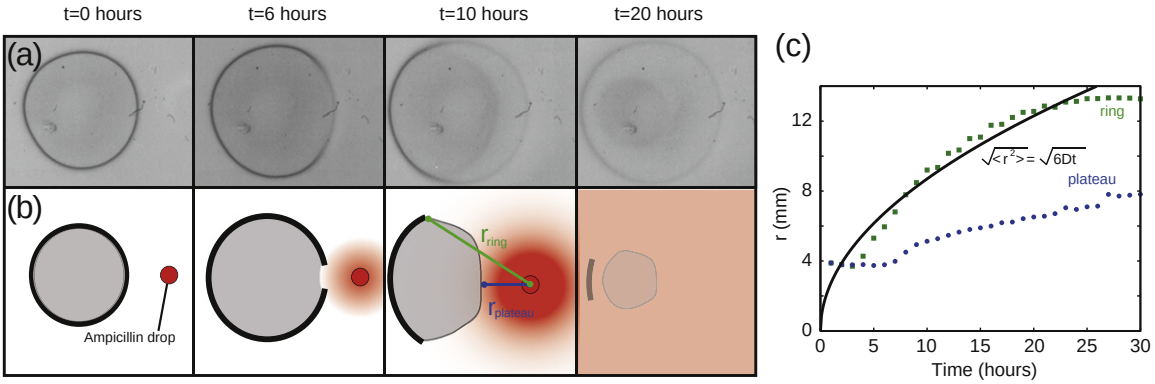

Fig. 6. Bacterial lysis by antibiotic in space and time shows differential rates of lysis. (a) At t=0 h, a small drop of ampicillin (3 µl of 100 mg/ml ampicillin, invisible) is placed 4 mm to the right of an expanding bacterial ring. At t=6 h, the ampicillin has reached the right edge of the ring and attenuates the bacterial density of the ring due to lysis of the bacteria. At t=10 h, ampicillin has diffused outward and lyses bacteria farther away from the source. The lysis front moves faster in the ring region than in the region of cells left behind the ring. Cells closest to the center are not lysed within the timescale of the experiment. (b) Schematic representation of the microscope images. The distance from the ampicillin drop to the advancing lysis front in the ring is denoted r_{ring}, and the distance to the advancing lysis front in the plateau is denoted $r_{plateau}$. (c) Dynamics of the lysis front shows how r_{ring} (green squares) and $r_{plateau}$ (blue circles) increase with time. The black continuous line is a plot (not a fit) of the root-mean-square of the distance ampicillin diffuses, given the previously measured diffusion constant $D=3.5\times10^{-6}\,cm^2/s$,[37] and corresponds roughly with the lysis front of the ring population. Note that, at each time point, the lysis front in the ring sees a lower level of ampicillin than the lysis front of cells behind the ring because of geometric considerations, and the fact that the concentration of a material diffusing from a source is a monotonically decreasing function of distance.

(exponential *versus* stationary phase), *galE* (the promoter of the *galETKM* operon,[33] required for galactose catabolism) and a promoter with a consensus site for the catabolite repressor protein CRP (*c*AMP *r*eceptor *p*rotein) levels.[28]

To prevent interference from the stationary population in the drop region, we measured the profile after the ring clearly separated. The two profiles showed that whereas the fluorescence profile from the CRP promoter showed high levels around the drop region relative to the levels at the peak (Fig. 5a), the fluorescence from the *fliC* promoter created a profile that was higher at the ring (Fig. 5b). We computed *s*, the ratio between the area under the curve in the ring region and the area under the curve in the drop region (Fig. 5c) and found that the fluorescence profile of *fliC* (blue bar) was increased in the ring 2-fold with respect to CRP (green bar) ($p<0.02$). From high to low values of *s*, the genes *galE*, *fliL*, *fliA* and σ_{70} lie in between *fliC* and CRP.

This result is similar to results obtained in swarm experiments on hyper-flagellated cells on hard agar, in which the extending tip of the swarm contains cells with the highest levels of flagellin.[34] Spatial regulation of gene expression has also been observed recently in *Bacillus subtilis* communities: the histidine kinases KinC and KinD were shown to be expressed mainly in the outer edges of the community, whereas KinA and KinB are expressed in the inner regions of the colony.[5]

Ring population is killed more effectively by antibiotic than the cells that stay behind

We finally asked what might be the physiological consequences of the spatial chemostat growth model, for example, with respect to surviving an antibiotic challenge. In particular, antibiotics such as ampicillin are well known to lyse growing cells more effectively than cells in stationary phase.[35] The spatial distibution of lysis can thus serve as an additional indicator for growth phases of the cells.

We added the antibiotic ampicillin in a small drop 4 mm outside the ring and measured where and when on the plate bacterial lysis occured. Ampicillin inhibits the enzyme transpeptidase required for the synthesis of cell walls of *E. coli*.[36] Using the present assay, we could track the lysis process in space and time. We found a lysis front that advanced in the ring region faster than in the region of cells left behind the ring (Fig. 6 and Supplemental Movie M1). Bacteria near the center, which have been in stationary phase the longest time, were lysed last.

The rapid advance of the lysis front in the ring occured despite the fact that antibiotic concentrations were lower: the ring lysis front was farther away from the source of diffusing antibiotic and, thus, saw lower concentrations at each time point than the lysis front of cells left behind the ring (i.e., $r_{ring}>r_{plateau}$ at all times) (Fig. 6). This is consistent with the

conclusion that cells in the chemotactic ring are growing faster, while bacteria in the "waste" have entered stationary phase.

Discussion

This study presented a microscopic assay for measuring *in situ* growth and gene expression in space and time, which was used to analyze the growth modes and gene expression of an expanding chemotactic bacterial population. As a model system, we used soft agar plates in which *E. coli* perform chemotaxis toward galactose. We found several new features of this process: (i) the chemotactic ring originates inside the inoculum and not at the edges and passes through the inoculum forcing cells behind into stationary phase, (ii) the ring concentration is constant with time and increases with the galactose concentration, (iii) the swim ring sheds cells behind forming a constant density plateau of non-growing cells, (iv) the density of the plateau relative to the ring is inversely proportional to the velocity of the ring and (iv) the swim ring shows elevated expression of flagellin (FliC) and metabolic enzymes galE. The results in this study support a model in which the growth of an advancing chemotactic population is analogous to a continuous culture in a chemostat. The growth rate is related to the chemotactic velocity, the spatial width of the population and the fraction of bacteria that the population leaves behind as it advances.

Bacterial biology has been frequently tested in chemostat conditions. The present study suggests that the chemostat is more than a useful tool for holding bacteria at constant conditions; it may be a good model for advancing motile populations. In a chemostat, the bacteria are held at the boundary between exponential and stationary phases—a phase that is passed very rapidly in batch culture but, based on the present study, may be relevant to spatially growing populations.

Our work is related to several other recent studies on migration of bacterial populations. Croze *et al.* employ soft agar plates and focus on the suppression of the combination of chemotaxis and diffusion as the gel concentration is increased, causing the expanding population to change width and shape from sharp rings to broad bands.[18] By overexpression of the flagellar sigma factor, we obtain modulation of the migration velocity due to chemotaxis only and focus on the mode of growth of the expanding population. Saragosti *et al.* studied travelling pulses of chemotactic bacteria in microchannels and show elegantly by single-bacterium tracking that bacteria swimming in the direction of the travelling pulse have a greater mean run length in comparison to those in the opposite direction.[17] Following the present work, the growth rate of the bacterial population inside the microchannels can be calculated, in principle, from the velocity and geometry of the pulse. Due to the fast travel velocity of the pulse, growth is of limited influence on the migration process, while in the present assay, growth is crucial.

We anticipate that chemostat-like growth might occur in other types of bacterial growth on surfaces, such as growth in colonies,[38,39] in biofilms and in swarming colonies.[34,40] Our finding that increasing the ring velocity decreases the "waste fraction" hints at a classic tradeoff in which swimming cells at the ring gain access to nutrients but are more susceptible to stresses such as antibiotics.[41] It would be interesting to explore how bacteria evolve to balance the competing tasks of rapid growth, rapid chemotaxis and survival. The present approach can be used to study bacterial growth and gene expression in a variety of situations where spatial effects are important.

Materials and Methods

Buffers and strains

E. coli K12 strain RP437 [*thr leu his metF eda rpsL thi ara lacY xyl tonA tsx*], WT for chemotaxis,[26] was transformed with the relevant reporter plasmid from a GFP-reporter library, in which promoter regions were fused to a fast-folding *gfpmut2* gene with a strong RBS (*r*ibosome *b*inding site).[21] For inducible expression of FliA, the *fliA* gene was cloned into pBAD18 and subsequently subcloned into pZA31. The araBAD promoter was used because of its low leakiness. Bacteria were grown in H1 medium,[42] containing D-(+)-galactose (Sigma-Aldrich), thiamine (1 μg/ml) and the four amino acids L-histidine, L-methionine, L-leucine and L-threonine (Calbiochem) that are required by RP437 for growth at a concentration of 250 μM each. Swim plates[43] contained 1.5 ml of (approximately 2 mm) of 0.15% (w/v) bactero agar (Pronadisa) and were covered with a thin layer (1.5 ml) of mineral oil (Sigma-Aldrich) to prevent evaporation.

Microscopy

A Leica DMI6000B inverted microscope was used with a Leica 5×/0.12 N PLAN objective and a Hamamatsu ORCA-ER CCD camera at 512×512 pixels. We used Costar 6-well cell culture plates as soft agar plates. Images were collected from an ~50-μm-deep plane below the surface of the soft agar plate where the bacteria swim. Polystyrene beads place on top of the gel were used to mark the surface of the gel. The entire stage was surrounded by an incubator set to 37 °C, allowing for the continuous observation of the soft agar plates without their removal from the incubator.

Image analysis of time-lapse movies

We used a custom-written image analysis program written in Matlab version 2011a (Mathworks). Field

correction was used to correct the raw images for non-uniform illumination (approximately 5% over the entire image) by dividing the raw image by the average image of the entire 169 image montage. The center of the ring was subsequently calculated from the transmission image by fitting a circle through the high bacterial density ring using the circfit routine. The image was then transformed to cylindrical coordinates with the calculated circle center as the origin. The transformed image was then divided into 200 equally spaced radial segments, which were averaged to yield the average radial profile. Finally, the background level was subtracted at each time point. The entire procedure was also applied for the fluorescence images. To obtain the number of bacteria in each radial segment, we calculated the integral in the relevant transmission segment, as described above.

Supplementary data to this article can be found online at http://dx.doi.org/10.1016/j.jmb.2012.09.005

Acknowledgements

We thank Erez Dekel, Nir Gov and Tziki Kam for discussions. We thank the Israel Science Foundation and the European Research Council (FP7/2007-2013/ERC Grant Agreement No. 249919) for support. D.A.K. thanks the Human Frontiers Science Project for a long-term postdoctoral fellowship.

Received 30 April 2012;
Received in revised form 2 September 2012;
Accepted 6 September 2012
Available online 20 September 2012

Keywords:
biofilms;
chemotaxis;
bacterial populations;
growth phases

References

1. Davidson, C. J. & Surette, M. G. (2008). Individuality in bacteria. *Annu. Rev. Genet.* **42**, 253–268.
2. Shapiro, J. A. (1998). Thinking about bacterial populations as multicellular organisms. *Annu. Rev. Microbiol.* **52**, 81–104.
3. Mendelson, N. H. & Salhi, B. (1996). Patterns of reporter gene expression in the phase diagram of *Bacillus subtilis* colony forms. *J. Bacteriol.* **178**, 1980–1989.
4. Budrene, E. O. & Berg, H. C. (1995). Dynamics of formation of symmetrical patterns by chemotactic bacteria. *Nature*, **376**, 49–53.
5. McLoon, A. L., Kolodkin-Gal, I., Rubinstein, S. M., Kolter, R. & Losick, R. (2011). Spatial regulation of histidine kinases governing biofilm formation in *Bacillus subtilis*. *J. Bacteriol.* **193**, 679–685.
6. Hall-Stoodley, L., Costerton, J. W. & Stoodley, P. (2004). Bacterial biofilms: from the natural environment to infectious diseases. *Nat. Rev., Microbiol.* **2**, 95–108.
7. Salhi, B. & Mendelson, N. H. (1993). Patterns of gene expression in *Bacillus subtilis* colonies. *J. Bacteriol.* **175**, 5000–5008.
8. Be'er, A., Ariel, G., Kalisman, O., Helman, Y., Sirota-Madi, A., Zhang, H. P. *et al.* (2010). Lethal protein produced in response to competition between sibling bacterial colonies. *Proc. Natl Acad. Sci. USA*, **107**, 6258–6263.
9. Berg, H. C. (2004). *E. coli* in Motion Springer-Verlag, New York, NY.
10. Adler, J. (1966). Chemotaxis in bacteria. *Science*, **153**, 708–716.
11. Kollmann, M., Lovdok, L., Bartholome, K., Timmer, J. & Sourjik, V. (2005). Design principles of a bacterial signalling network. *Nature*, **438**, 504–507.
12. Liu, C., Fu, X., Liu, L., Ren, X., Chau, C. K., Li, S. *et al.* (2011). Sequential establishment of stripe patterns in an expanding cell population. *Science*, **334**, 238–241.
13. Ames, P. & Parkinson, J. S. (2007). Phenotypic suppression methods for analyzing intra- and intermolecular signaling interactions of chemoreceptors. *Methods Enzymol.* **423**, 436–457.
14. Landman, K. A., Simpson, M. J., Slater, J. L. & Newgreen, D. F. (2005). Diffusive and chemotactic cellular migration: smooth and discontinuous traveling wave solutions. *SIAM J. Appl. Math.* **65**, 1420–1442.
15. Nadin, G., Perthame, B. & Ryzhik, L. (2008). Traveling waves for the Keller–Segel system with Fisher birth terms. *Interfaces and Free Boundaries*, **10**, 517–538.
16. Saragosti, J., Calvez, V., Bournaveas, N., Buguin, A., Silberzan, P. & Perthame, B. (2010). Mathematical description of bacterial traveling pulses. *PLoS Comput. Biol.* **6**, e1000890.
17. Saragosti, J., Calvez, V., Bournaveas, N., Perthame, B., Buguin, A. & Silberzan, P. (2011). Directional persistence of chemotactic bacteria in a traveling concentration wave. *Proc. Natl Acad. Sci. USA*, **108**, 16235–16240.
18. Croze, O. A., Ferguson, G. P., Cates, M. E. & Poon, W. C. (2011). Migration of chemotactic bacteria in soft agar: role of gel concentration. *Biophys. J.* **101**, 525–534.
19. Tindall, M. J., Maini, P. K., Porter, S. L. & Armitage, J. P. (2008). Overview of mathematical approaches used to model bacterial chemotaxis II: bacterial populations. *Bull. Math. Biol.* **70**, 1570–1607.
20. Wolfe, A. J. & Berg, H. C. (1989). Migration of bacteria in semisolid agar. *Proc. Natl Acad. Sci. USA*, **86**, 6973–6977.
21. Zaslaver, A., Bren, A., Ronen, M., Itzkovitz, S., Kikoin, I., Shavit, S. *et al.* (2006). A comprehensive library of fluorescent transcriptional reporters for *Escherichia coli*. *Nat. Methods*, **3**, 623–628.
22. Lapidus, I. R. & Schiller, R. (1978). A model for traveling bands of chemotactic bacteria. *Biophys. J.* **22**, 1–13.
23. Keller, E. F. & Segel, L. A. (1971). Traveling bands of chemotactic bacteria: a theoretical analysis. *J. Theor. Biol.* **30**, 235–248.

24. Novick, A. & Szilard, L. (1950). Description of the chemostat. *Science*, **112**, 715–716.
25. Lutz, R. & Bujard, H. (1997). Independent and tight regulation of transcriptional units in *Escherichia coli* via the LacR/O, the TetR/O and AraC/I1-I2 regulatory elements. *Nucleic Acids Res.* **25**, 1203–1210.
26. Parkinson, J. S. (1978). Complementation analysis and deletion mapping of *Escherichia coli* mutants defective in chemotaxis. *J. Bacteriol.* **135**, 45–53.
27. Dekel, E. & Alon, U. (2005). Optimality and evolutionary tuning of the expression level of a protein. *Nature*, **436**, 588–592.
28. Kaplan, S., Bren, A., Zaslaver, A., Dekel, E. & Alon, U. (2008). Diverse two-dimensional input functions control bacterial sugar genes. *Mol. Cell*, **29**, 786–792.
29. Malakooti, J., Ely, B. & Matsumura, P. (1994). Molecular characterization, nucleotide sequence, and expression of the *fliO*, *fliP*, *fliQ*, and *fliR* genes of *Escherichia coli*. *J. Bacteriol.* **176**, 189–197.
30. Mytelka, D. S. & Chamberlin, M. J. (1996). *Escherichia coli fliAZY* operon. *J. Bacteriol.* **178**, 24–34.
31. Koo, B. M., Rhodius, V. A., Campbell, E. A. & Gross, C. A. (2009). Mutational analysis of *Escherichia coli* σ^{28} and its target promoters reveals recognition of a composite −10 region, comprised of an "extended −10" motif and a core −10 element. *Mol. Microbiol.* **72**, 830–843.
32. Aldridge, P. & Hughes, K. T. (2002). Regulation of flagellar assembly. *Curr. Opin. Microbiol.* **5**, 160–165.
33. Weickert, M. J. & Adhya, S. (1993). The galactose regulon of *Escherichia coli*. *Mol. Microbiol.* **10**, 245–251.
34. Hamze, K., Autret, S., Hinc, K., Laalami, S., Julkowska, D., Briandet, R. *et al.* (2011). Single-cell analysis in situ in a *Bacillus subtilis* swarming community identifies distinct spatially separated subpopulations differentially expressing hag (flagellin), including specialized swarmers. *Microbiology*, **157**, 2456–2469.
35. Tuomanen, E., Cozens, R., Tosch, W., Zak, O. & Tomasz, A. (1986). The rate of killing of *Escherichia coli* by beta-lactam antibiotics is strictly proportional to the rate of bacterial growth. *J. Gen. Microbiol.* **132**, 1297–1304.
36. Costerton, J. W., Stewart, P. S. & Greenberg, E. P. (1999). Bacterial biofilms: a common cause of persistent infections. *Science*, **284**, 1318–1322.
37. Lehmenkuhler, A., Kersting, U. & Nicholson, C. (1988). Diffusion of penicillin in agar and cerebral cortex of the rat. *Brain Res.* **444**, 181–183.
38. Hallatschek, O., Hersen, P., Ramanathan, S. & Nelson, D. R. (2007). Genetic drift at expanding frontiers promotes gene segregation. *Proc. Natl Acad. Sci. USA*, **104**, 19926–19930.
39. Shapiro, J. A. (1987). Organization of developing *Escherichia coli* colonies viewed by scanning electron microscopy. *J. Bacteriol.* **169**, 142–156.
40. Kearns, D. B. & Losick, R. (2003). Swarming motility in undomesticated *Bacillus subtilis*. *Mol. Microbiol.* **49**, 581–590.
41. Shoval, O., Sheftel, H., Shinar, G., Hart, Y., Ramote, O., Mayo, A. *et al.* (2012). Evolutionary trade-offs, Pareto optimality, and the geometry of phenotype space. *Science*, **336**, 1157–1160.
42. Hazelbauer, G. L., Mesibov, R. E. & Adler, J. (1969). *Escherichia coli* mutants defective in chemotaxis toward specific chemicals. *Proc. Natl Acad. Sci. USA*, **64**, 1300–1307.
43. Adler, J. (1976). Chemotaxis in bacteria. *J. Supramol. Struct.* **4**, 305–317.